Journal of Natural Gas Science and Engineering xxx (2017) 1–11

Contents lists available at ScienceDirect

Journal of Natural Gas Science and Engineering

journal homepage: www.elsevier.com/locate/jngse

The impact of kerogen properties on shale gas production: A reservoir simulation sensitivity analysis

Shihao Wang [a, b, *], Andrew E. Pomerantz [b], Wenyue Xu [b], Alexander Lukyanov [b], Robert L. Kleinberg [b], Yu-Shu Wu [a]

[a] Department of Petroleum Engineering, Colorado School of Mines, Golden, CO 80401, United States
[b] Schlumberger-Doll Research, Cambridge, MA 02139, United States

ARTICLE INFO

Article history:
Received 1 October 2016
Received in revised form
19 March 2017
Accepted 10 June 2017
Available online xxx

Keywords:
Shale gas simulation
Kerogen structure
Triple porosity model
Slippage effect

ABSTRACT

Gas shales are complex materials with transport occurring over many length scales, from relatively large systems such as natural and induced fractures to relatively small systems including kerogen-hosted pores of nearly molecular size. Here we present results of a sensitivity analysis performed using reservoir simulation designed to test how these different pore space length scales impact gas production. The shale is modeled as a triple porosity system comprising: first, natural and induced fractures; second, kerogen-hosted pores of approximately 25 nm diameter (as are typically observed in SEM images); and third, kerogen-hosted pores of approximately 1 nm diameter (which are below the size detectable by SEM but are typically observed in X-ray diffraction and gas adsorption experiments). In these simulations, the smaller kerogen-hosted pores act as a source term, releasing primarily adsorbed gas. The larger kerogen-hosted pores contribute to storage and transport, serving both as a source of gas on their own and a system through which the gas originating in the smaller pores can flow. As a result, the volume of the smaller pores impacts mainly the later production, when the reservoir pressure is near or below the Langmuir pressure. The volume of the larger pores impacts mainly the early stage of production, when mainly free gas is being produced. The radius of the smaller pores impacts the late stage of production, as smaller pores have greater surface area and therefore larger Langmuir volume. The radius of the larger pores has little impact on the ultimate recovery but instead impacts the production rate, as larger pores correlate with greater permeability. The results suggest that measurements of the variation of kerogen properties—performed potentially using cuttings, cores, or logs—can be used to refine parameters in reservoir simulations.

1. Introduction

Shale formations are a rich resource of natural gas, and reservoir simulation is a power tool to predict the production of shale gas reservoirs. In order to conduct accurate shale gas reservoir simulation, a precise model of the structure of shale rock is critical. The solid matrix of shale consists of organic components (kerogen) and inorganic components (minerals). The inorganic matter makes little contribution to overall gas conductivity (Ambrose et al., 2012), while the organic matter is permeable and is the actual source of trapped gas.

In the literature, many researchers have looked at the pore structures of shale formations and the associated transport mechanisms of shale gas (Zhang et al., 2012a,b,c). studied the effects of organic-matter type on the transport mechanism of methane in shale formation (Jarvie et al., 2007). investigated the formation of kerogen and reviewed the complexity of its pore structure from a geological perspective (Ambrose et al., 2010). brought out a novel pore-scale model to account for different types of pores in the shale rock (Wang et al., 2017a,b,c). proposed a delayed adsorption diffusion model to quantify the adsorption process in the kerogen of shale formations. Their results indicate that the free gas and then desorption of adsorbed gas mainly contributes to early and late stage of production respectively. Recently (Wang et al., 2017a,b,c), thoroughly reviewed the transport mechanism in shale as well as tight sandstone formations.

Several experiments and observations (Falk et al., 2015;

* Corresponding author. Department of Petroleum Engineering, Colorado School of Mines, Golden, CO 80401, United States.
E-mail address: gohych@gmail.com (S. Wang).

http://dx.doi.org/10.1016/j.jngse.2017.06.009
1875-5100/

Gensterblum et al., 2015) have indicated that the organic matter consists of complex pore networks. On one hand, relatively larger pores with diameter up to hundreds nanometers are observed by scanning electron microscope (SEM). On the other hand, pores too small to be observed by SEM have been discovered through numerical reconstruction of kerogen structure from measurements such as by X-ray and neutron diffraction (Bousige et al., 2016; Ho et al., 2016). The triple-porosity characteristic of shale has also been reported by (Wang et al., 2017a,b,c).

Due to the special features of shale formations, the reservoir simulation models that has been used successfully in conventional reservoirs fail to predict the behaviors of shale reservoirs correctly, as reported by (Cipolla et al., 2010). Specifically, on the simulation of shale matrix, it has been reported (Yan et al., 2016a,b) that the traditional dual porosity model fails to accurately represent shale formation. Therefore, a new model should be developed for the simulation of shale gas reservoirs (Pruess, 1985). brought out the Multiple Interacting Continua (MINC) model for fractured reservoirs, which subdivides the rock matrix into nested continuum (Yan et al., 2016a,b). adopts the concepts of multiple porosity model and subdivides the shale formation based on the transport mechanism of shale gas. The above mentioned work provides useful inspiration on the modeling of shale matrix, however, none of them accounts for the recent discoveries of the nano-pore system inside kerogen.

In this work, we propose to use a triple porosity model to more accurately simulate shale gas reservoirs. The triple porosity model considers fractures, relatively large kerogen-hosted pores (such as observed by SEM), and relatively small kerogen-hosted pores (such as observed by X-ray and neutron diffraction). The larger kerogen-hosted pores, connected with the fractures, play the role as a flow pathway with higher permeability, while the smaller kerogen-hosted pores with adsorbed gas inside are the 'source' term, which supports the flow in the larger pores. In this way, the fractures, the larger pores and the smaller pores form a triple porosity system. Compared to the existing dual porosity model, this triple porosity model is a more realistic description of shale rocks.

Gas flow inside shale matrix is modeled using a gas apparent permeability correlation developed previously (Xu et al., 2015). The correlation is capable of capturing both the slippage velocity effect and the diffusion process inside shale. In this work, the correlation is implemented in the ECLIPSE simulator (Sclumberger, 2010) and sensitivity analyses are conducted on the triple porosity model. Sensitivity analysis are conducted on several parameters in the simulation, including the permeability, the porosity, the shape factor and the adsorption capability. The purpose is to examine the roles of absorbed gas, large-pore system and the small-pore system play during different stages of the shale gas production.

This papers is organized as follows: in the next section, the mathematical and physical background of the problem is introduced. In Section 3, the novel triple porosity model is described, as are the results of the sensitivity analyses. In the last section, conclusions regarding the impact of these different pore systems on gas production are presented.

2. Methodology

2.1. Mathematical model

The compositional modeling module of the reservoir simulator ECLIPSE is used to study the shale gas problem. The reservoir is assumed to contain only methane gas. In ECLIPSE, the mass conservation for single phase single component is as follows:

$$\frac{\partial M}{\partial t} = \nabla \cdot \vec{F} + q \tag{2.1}$$

In the above equation, M is the accumulation term of methane, F is the mass flux, q is the sink/source term.

Since throughout this work considers only single-phase gas flow, the accumulation term includes the free and adsorbed gas, as follows

$$M = \phi\rho + m_a \tag{2.2}$$

where ϕ is the porosity, ρ is the free gas density, m_a is the adsorption term. The mass flux $\vec{F}$ is given by the Darcy's law

$$\vec{F} = -K_a \frac{\rho}{\mu}(\nabla P - \rho \vec{g}) \tag{2.3}$$

In the above equation, K_a is the apparent permeability that is corrected from the absolute permeability of the rock, to account for the gas slippage effect (Klinkenberg effect), $\vec{g}$ is the gravitational acceleration, μ is gas phase viscosity. Peng-Robinson equation of state (Peng and Robinson, 1976) is used to calculated the gas phase properties. ECLIPSE uses molar densities of each component as the primary variables. In the current case, only methane present in the system, therefore the molar density is equivalent to the mass fraction. Equation (2.1) is solved by the finite volume method in time-space domain. The details of the numerical approach can be found in (Sclumberger, 2010).

2.2. Permeability enhancement effect

It is believed that the permeability enhancement effect in the nano-pores of unconventional formation results from the 'slippage' of gas flow. The slippage effect can be explained by kinetic theory of gases. In the nano-pore system, gas molecules keep moving randomly, which is defined as the thermodynamic motion. When a gas molecule collides with the wall of the pore, the reflection will be either specular or diffuse. Specular reflection keeps the horizontal component of its previous flux velocity, and no horizontal component of its momentum is lost during the process of the collision. However, in diffuse reflection, the molecule will reflect into a random direction and its previous momentum is lost. The ratio of diffuse reflection among collision is defined as the tangential momentum accommodation coefficient (Agrawal and Prabhu, 2008; Chew, 2009), varying from 0 to 1 (Knudsen, 1909, 1934). found it being 1 based on his experiments. The current consensus is between 0.9 and 1 depending on the wall roughness and molecule type (Kleinstreuer and Koo, 2004; Zhang et al., 2012a,b,c), as summarized by (Zhang et al., 2012a,b,c). The loss of momentum induced by diffuse reflection is the cause of gas 'slippage' along pore walls. Meanwhile, the reflected molecules contribute to molecular diffusion process. Such effect is called the Knudsen diffusion. The apparent permeability enhancement results from the combined effect of velocity slippage and Knudsen diffusion, as shown in Fig. 1.

The gas slippage effect can be expressed in the following equation.

$$u_{slip} = C \cdot \lambda \left(\frac{\partial u}{\partial n}\right)_s \tag{2.4}$$

In the above equation, u_{slip} is the slippage velocity. $(\partial u/\partial n)_s$ is the first order of flux velocity derivative at the wall. C is a constant. λ is the mean free path of gas, expressed in the following equation

$$\lambda = \frac{m}{\sqrt{2}\pi\delta^2\rho} \tag{2.5}$$

where δ is the collision diameter of the molecules and m is the

Please cite this article in press as: Wang, S., et al., The impact of kerogen properties on shale gas production: A reservoir simulation sensitivity analysis, Journal of Natural Gas Science and Engineering (2017), http://dx.doi.org/10.1016/j.jngse.2017.06.009

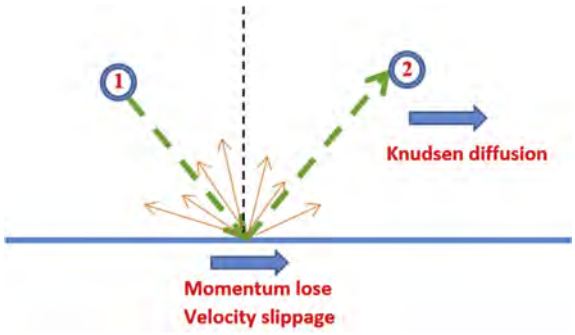

Fig. 1. Combined effect of velocity slippage and Knudsen diffusion (Wang et al., 2017a,b,c).

molecular weight. ρ is the density of the gas.

Here we should mention that the slippage velocity can be the higher order functions of the velocity derivative. Meanwhile, C can not only be a constant but also a function of the Knudsen number K_N, defined as the ratio between the mean free path of gas and the diameter of the pore (Zhang et al., 2012a,b,c). has thoroughly reviewed and summarized existing slippage conditions. In this work, we use the first-order slippage condition proposed by (Maxwell, 1879), as follows

$$u_{slip} = \frac{2}{3}\frac{2-\sigma_s}{\sigma_s}\cdot\lambda\left(\frac{\partial u}{\partial n}\right)_s \tag{2.6}$$

where σ_s is the tangential accommodation momentum coefficient (TMAC).

The Knudsen diffusion effect can be quantified by the Knudsen diffusion coefficient, as follows

$$D_0 = \frac{m}{\pi\delta^2}\sqrt{\frac{p}{6\rho^3}} \tag{2.7}$$

As mentioned above, the slippage effect and the Knudsen diffusion effect co-exist in the nano-pores. Therefore, in this work, we use a transport mechanism model that combines both of the two effects. The model is internally developed by Schlumberger and has been briefly described by (Xu et al., 2015). In the transport model, both gas slippage effect and Knudsen diffusion process are taken into consideration. In the vicinity of the boundary (wall) of the flow channel is the Knudsen layer. The thickness of the Knudsen layer is 2/3λ, which can be calculated from kinetic theory of gases (Present, 1958). Inside the Knudsen layer, Knudsen diffusion is the major transport process. Because of the slippage effect, the velocity of the Knudsen layer is no more zero but the velocity calculated from Equation (2.6). The viscous bulk flow, subject to shear stress, is the middle part of the flow channel.

The above process can be quantitatively viewed as a permeability enhancement effect of gas phase. In this work, we express the model as

$$K_a = S(K_N)K_\infty \tag{2.8}$$

where K_a is the apparent permeability and K_∞ is the absolute permeability, S is the permeability multiplier, and K_N is the Knudsen number.

According to this model, when Knudsen number is greater than 0.75, the viscous bulk flux disappears and Knudsen diffusion becomes the only transport process. In this sense, at low Knudsen number range (larger pores), gas slippage effect is the dominant transport mechanism; while at high Knudsen number range (smaller pores), Knudsen diffusion is the dominant transport mechanism. It can been seen from above that this model is non-empirical and is derived from first principals of hydrodynamics. Gas properties from NIST database (Ralchenko et al., 2010) are used in the model. It should be noted that these results can also be quantitatively obtained by other permeability enhancement correlations, such as (Ertekin et al., 1986; Tang et al., 2005).

2.3. Adsorption effect

The organic matter inside shale (kerogen) can trap large amounts of gas by adsorption. The adsorption behavior of shale is typically quantified by the Langmuir isotherm (Langmuir, 1918), shown as follows.

$$V = V_L\frac{P}{P+P_L} \tag{2.9}$$

where V_L is the Langmuir volume that determines the maximum volume of adsorbed gas, while P_L is the Langmuir pressure. If pressure P equals to P_L, the volume of adsorption gas V is just half of the Langmuir volume. By assuming the pore system consists of long capillary tubes, it can be shown that the surface area of the organic matter is proportional to the porosity while inversely proportional to the pore radius, as

$$A \propto \frac{\phi}{r} \tag{2.10}$$

In the above formulation, A is the surface area, ϕ is the porosity and r is the pore radius of the organic matter. From the above formulation, the narrower the pore is, the more surface area is available for gas adsorption. Based on Equation (2.6), the relationship between Langmuir volume and pore radius can be described as

$$\frac{V_L}{V_{L0}} = \frac{r_0}{r} \tag{2.11}$$

In this way, the Langmuir volume, V_L, for pore radius r can be calculated from a reference Langmuir volume V_{L0} and reference pore radius r_0.

(Heller and Zoback, 2014) conducted experiments to determine the Langmuir volume and Langmuir pressure on shale samples from several reservoirs. Their data shows that the adsorption parameters largely vary among different reservoirs. However, typically the Langmuir pressure is 500 psi (3.5 MPa) to 1500 psi (10.5 MPa) and the Langmuir volume is 10 scf/ton (0.00028 m^3/kg) to 100 scf/ton (0.0028 m^3/kg). The typical curves of the Langmuir isotherm are plotted in Fig. 2 and Fig. 3.

3. Triple porosity model

As shown by the left side of Fig. 4 (SEM image of a typical shale), the organic matter consists of a complex pore network. A more detailed SEM image of the organic matter is shown on the right of Fig. 4. The diameter of pores shown in Fig. 4 is between several dozens to hundreds nanometers. Furthermore, according to a recent work (Bousige et al., 2016; Falk et al., 2015; Ho et al., 2016), there are a large number of smaller pores beyond the resolution of SEM that are not shown in Fig. 4. To characterize such pore system, the multiple porosity approach is more suitable than the dual porosity approach. In this work, we propose the usage of the triple porosity approach. In the triple porosity model, the first porosity system is the hydraulic/natural fractures, which connect the matrix rock and the production well. The second system and the third system are modeled by dividing the organic matter of the shale

Please cite this article in press as: Wang, S., et al., The impact of kerogen properties on shale gas production: A reservoir simulation sensitivity analysis, Journal of Natural Gas Science and Engineering (2017), http://dx.doi.org/10.1016/j.jngse.2017.06.009

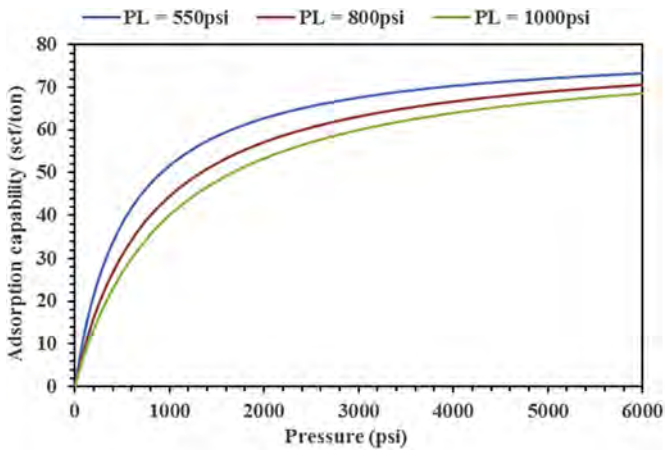

Fig. 2. Langmuir isotherm with different Langmuir pressure (temperature = 373 K/212 °F, Langmuir volume = 80 scf/ton).

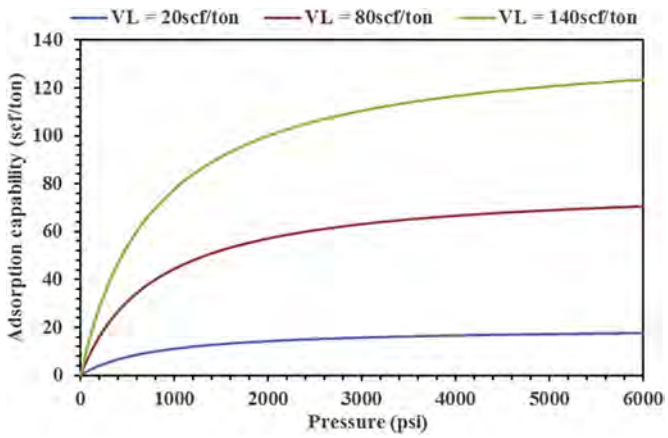

Fig. 3. Langmuir isotherm with different Langmuir volume (temperature = 373 K/212 °F, Langmuir pressure = 800 Psi).

matrix into two parts: the large-pore system with wider pores and the small-pore system with narrower pores. The large-pore system plays the role as a flow pathway for the gas molecules to move from the organic matter into the fractures, while the small-pore system with adsorbed gas serves as a 'source', supporting the flow inside the larger pores. Inorganic-hosted pores are believed to be typically saturated with water (Li et al., 2016) and therefore make little contribution to gas transport, so those pores are neglected here. According to the previous discussion, inside the smaller pores, Knudsen diffusion is the dominant transport mechanism. Inside the larger pores, gas slippage effect (with Darcy's flow) is the dominant transport mechanism. Inside the mirco-cracks, Darcy's flow is the dominant transport mechanism. The conceptual model of the triple porosity system is shown in Fig. 5.

The single phase flow coming out from porosity system i into porosity system j is numerically calculated by

$$q = \sigma \frac{K_a \rho}{\mu} A(P_i - P_j) \tag{3.1}$$

In the above equation, ρ and μ are the density and viscosity of the gas phase respectively, σ is a 'shape factor', that is only dependent on the geometry of the grid block i, K_a is the apparent permeability of gas phase of the porosity in the inner side (with lower permeability). In conventional reservoir simulation, the shape factor has been extensively investigated (Kazemi et al., 1976; Lim and Aziz, 1995; Wang et al., 2016; Warren and Root, 1963; Zimmerman et al., 1993). The shape factor can be derived from analytical or semi-analytical approaches, based on the concept of 'characteristic length', which is used to represent is the length scale of the porous network from which hydrocarbon molecules are transported into the next-level pore or fracture network. According to (Warren and Root, 1963), the shape factor is defined as

$$\sigma = \frac{4N(N+2)}{L^2} \tag{3.2}$$

In the above equation, L is the characteristic length and N is the number of fracture sets surrounding the matrix. In this work, N is chosen to be 3 for the shape factor between the small-pore system and the large-pore system, because of the sparse nature of the nano-pore flow channels, and N is chosen to be 1 for the shape factor between the large-pore system and the fracture, since the simulation includes only one large fracture, as shown in Fig. 7. The shape factor concept has been successfully used in conventional reservoir simulation. However, in unconventional reservoirs, the shape factor has not been fully studied, especially for the shape factor between the porosity systems inside the matrix. To be specific, the characteristic length of the small-pore system is not clear yet. Therefore, in this work, a sensitivity analysis is conducted on the shape factor between the small-pore system and the large-pore system.

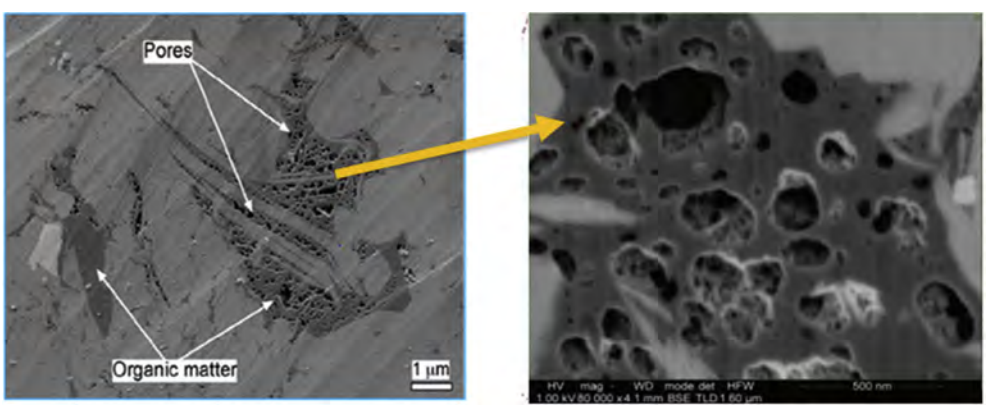

Fig. 4. SEM picture showing the pore structure of shale (Curtis et al., 2010; Yan et al., 2016a,b).

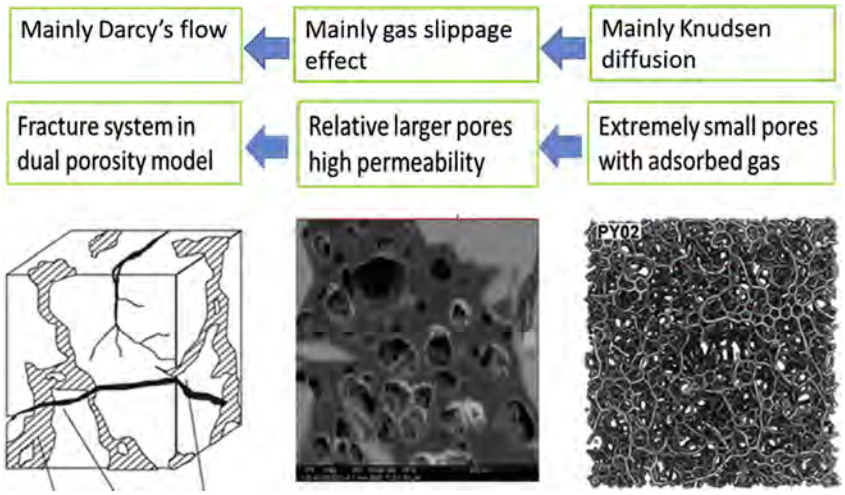

Fig. 5. Conceptual model of the triple porosity system (Bousige et al., 2016; Curtis et al., 2010).

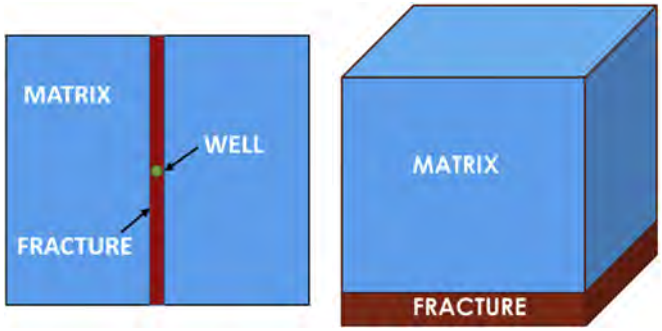

Fig. 6. Conceptual model of the reservoir scale case. Left: the reservoir. Right: the model used in simulation.

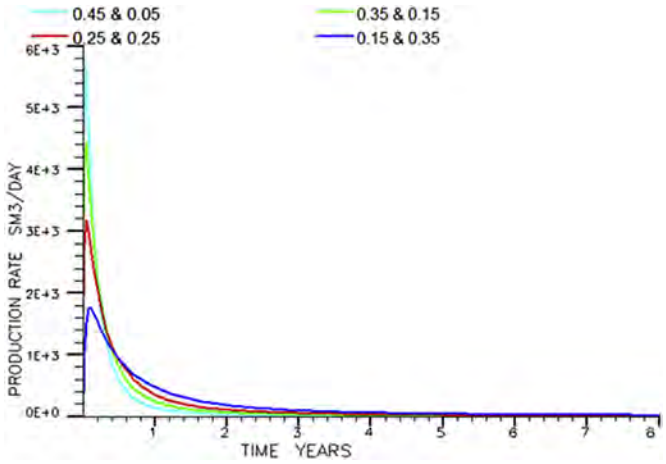

Fig. 7. Methane production rate with different combinations of the porosity of the two pore system. The first value in each legend is the porosity of the large-pore system of the organic matter, while the second value in each legend is the porosity of the small-pore system of the organic matter. Bulk rock porosity is 0.05 in all cases.

4. Case study and sensitivity analysis

In this section, we conduct reservoir scale case studies to investigate the sensitivity of shale gas production to several parameters including porosity, permeability and pore radius of the different pore systems.

4.1. Problem description

The conceptual model of the base case is shown in Fig. 6. On the left of Fig. 6 is the top view of the stimulated reservoir volume (SRV) of a shale gas reservoir with a well in the center. On the right of Fig. 6 is the numerical model, which is a 'quarter' of the reservoir. Because the problem is symmetric, the numerical model should be an accurate representation of the reservoir. The problem is simulated by the triple porosity model as described in Sections 2 and 3. The reservoir is initially saturated with methane gas. A well produces at a constant bottom hole pressure for 12 years. The input parameters for the base case are listed in Table 1. We conduct sensitivity analysis on the input parameters and record the methane production rate and the cumulative production for each case. In the base case presented here, the average diameter of larger pores of the shale system is set to 25 nm, while that of the smaller pores is set to 1 nm and the porosity of each system is set to 25%. The numbers represent the approximate averages of results presented from SEM imaging as well as from X-ray and neutron diffraction (Bousige et al., 2016; Wang et al., 2017a,b,c). The absolute permeability of the two porosity system can be thus estimated from their pore diameters.

Table 1
Input parameters of the base case for the sensitivity analysis.

Properties	Values	Units
Fracture network (effective) permeability	3.0	mD
Fracture network (effective) porosity	2.5e-4	dimensionless
Large-pore system permeability	10	μD
Large-pore system porosity	0.25	dimensionless
Shape factor to fractures	0.048	m^{-2}
Larger pore radius	25	nm
Large-pore system volume fraction	10%	dimensionless
Small-pore system permeability	5	nD
Small-pore system porosity	0.25	dimensionless
Smaller pore radius	1	nm
Small-pore system volume fraction	10%	dimensionless
Langmuir pressure	1000	psi
Shape factor to large-pore system	0.06	μm^{-2}
Langmuir volume	60	scf/ton
Reservoir temperature	212 (100)	°F (°C)
Reservoir initial pressure	4000	psi
Bottom hole pressure	1000	psi

Please cite this article in press as: Wang, S., et al., The impact of kerogen properties on shale gas production: A reservoir simulation sensitivity analysis, Journal of Natural Gas Science and Engineering (2017), http://dx.doi.org/10.1016/j.jngse.2017.06.009

4.2. Sensitivity analysis of porosity of the large and small kerogen-hosted pores

In this section, we conduct sensitivity analysis on the porosity of the shale. Several cases are run with different combinations of porosity of the large-pore system and the small-pore system. In each case, the total volume of the organic matter is 10% of the matrix volume and the total porosity is set to be 0.05. All combinations of the porosity are shown in Table 2. The absolute permeability for the larger pores is calculated from Aguilera's correlation (Aguilera, 2002). The production rate curves are shown in Fig. 7. As shown by Fig. 7, if the large-pore system has higher porosity, the production rate is higher in the early stage, because the large-pore system contains free gas and directly connects with the fracture. Therefore, if the porosity of the large-pore system is higher, there will be more gas stored inside the larger pores that flows into the fracture as well as the well at the early stage of the production. The early stage production rate is almost proportional to the absolute permeability. On the other hand, if the small-pore system has high porosity, more gas will flow into the fracture at the late stage of the production. Meanwhile, as the small-pore system contains primarily adsorbed gas, the porosity of the smaller pore affects the amount of the adsorbed gas. This is better indicated by the cumulative production curves shown in Fig. 8. As can be seen from Fig. 8, the cumulative production of cases with more small pores will exceed that of those with more large pores at the late stage of production. The total amount of gas produced by cases with more small pores is also higher than cases with more large pores. Thus, accurate characterization of the pore structures of shale is of great importance to the simulation of shale gas production. Our results are consistent with the observations of (Yang et al., 2015), which also show that different pore systems dominant different stages of production.

4.3. Sensitivity analysis of pore radius

4.3.1. Pore radius for small-pore system

As mentioned above, the pore radius has several effects on the fluid flow inside shale formation. Firstly, according to Aguilera's correlation, pore radius is related with the absolute permeability of rocks. Rocks with wider pores are more permeable. Secondly, as described by the permeability multiplier, if the pore becomes smaller, the Knudsen number will become larger and the Knudsen effect (permeability enhancement effect) becomes more significant. Thirdly, as shown in the previous section, the amount of adsorbed gas is inversely proportional to the pore radius. In this section, we conduct sensitivity analysis on the pore radius of the large-pore system and the small-pore system respectively. The pore radius, the absolute permeability and the Langmuir volume of the small-pore systems are listed in Table 3. The Langmuir volume is calculated from Equation (2.11). The other parameters are still chosen as the base case as shown in Table 1.

The permeability multiplier with respect to reservoir pressure of the three different types of smaller pores is shown in Fig. 9, from

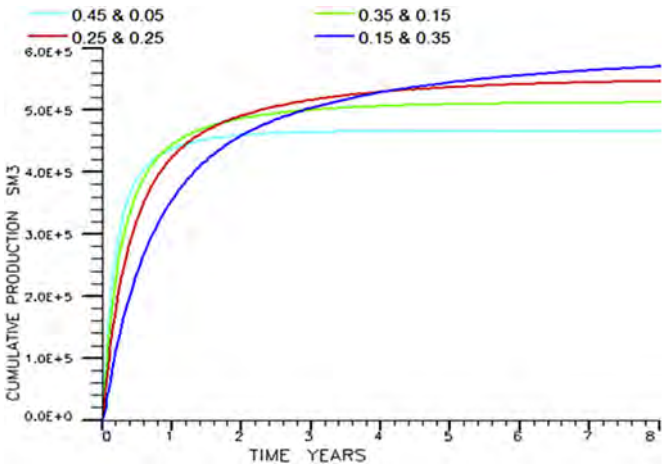

Fig. 8. Methane cumulative production with different combinations of the porosity of the two pore system.

Table 3
Parameters related to pore radius for the small-pore system.

Case index	Pore radius	Absolute permeability	Langmuir volume
5	1 nm	2 nd	60 scf/ton
6	3 nm	18 nd	20 scf/ton
7	5 nm	50 nd	12 scf/ton

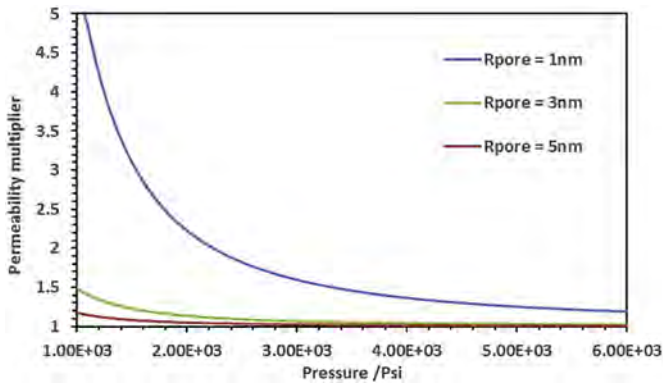

Fig. 9. Permeability multiplier for different pore radius of the small-pore system.

which we can see that the permeability is very sensitive to the pore radius of the small-pore system, especially in the low pressure zone that is close to the wellbore. The apparent permeability curves of the three cases are plotted in Fig. 10. According to Fig. 10, as the pore radius decreases, the permeability enhancement effect becomes more significant. For example, the absolute permeability of Case 5 (1 nm) is 1/25 of that of Case 7. After taking the permeability enhancement effect into consideration, the above ratio becomes 1/5 in the wellbore range.

Table 2
Porosity combination of the large-pore system and the small-pore system.

Case index	Porosity for larger pores (organic matter only)	Absolute permeability for larger pores (μd)	Porosity for smaller pores (organic matter only)	Total porosity
1	0.45	18	0.05	0.05
2	0.35	14	0.15	0.05
3	0.25	10	0.25	0.05
4	0.15	6	0.35	0.05

Please cite this article in press as: Wang, S., et al., The impact of kerogen properties on shale gas production: A reservoir simulation sensitivity analysis, Journal of Natural Gas Science and Engineering (2017), http://dx.doi.org/10.1016/j.jngse.2017.06.009

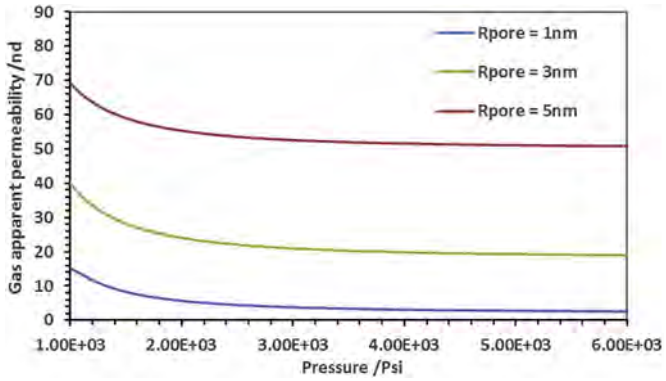

Fig. 10. Gas apparent permeability for different pore radius of the small-pore system.

The methane production rate and the cumulative production curves are shown in Fig. 11and Fig. 12 respectively. The small-pore system starts to affect the production at the late stage of the production. During the early stage of the production, because the small-pore system is not directly connected with the fractures and the reservoir pressure greatly exceeds the Langmuir pressure, the small-pore system contributes little production and the production curve of the three cases are almost the same. After a certain time, when the initial gas inside the fractures as well as large pores is mostly depleted, the small-pore system starts to support the production by feeding the flow inside the large-pore system as well as the fractures. As shown by Fig. 11, the production rate is not very sensitive to the radius of the small-pore system. This is because that the apparent permeability of the small pore is very low and the gas inside them propagates extremely slowly. However, as indicated by Fig. 12, the cumulative production is more sensitive to the pore radius of the small pores. As the pore radius of the small-pore system decreases, the eventual amount of gas produced increases significantly. The reason is that if the amount of adsorbed gas is inversely proportional to the radius of the nanopores. Therefore, given the same porosity, the smaller the pores are, the more the initial gas in place there is. Our observation is also consistent with that of (Wang et al., 2017a,b,c), who observed experimentally that desorption process contributes to the latter stage of production.

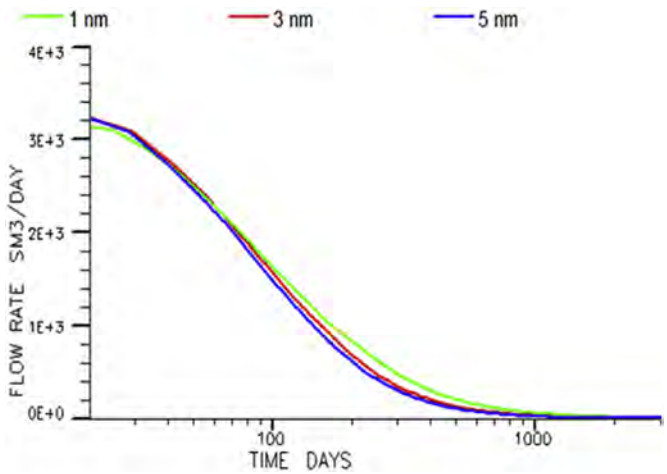

Fig. 11. Methane production rate with respect to time for different radius of the smaller pores.

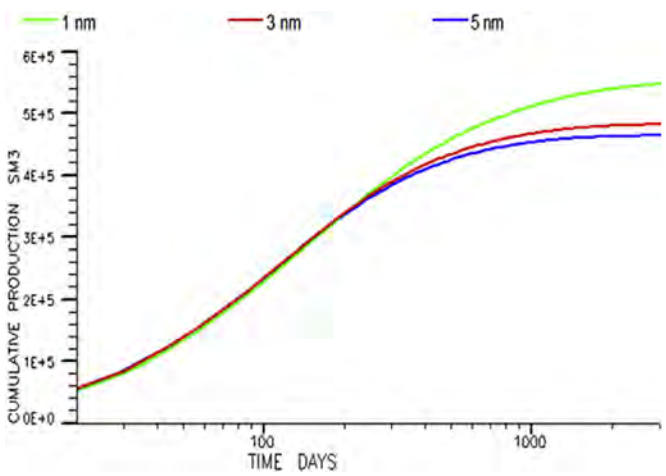

Fig. 12. Methane cumulative production with respect to time for different radius of the smaller pores.

4.3.2. Pore radius for the large-pore system

In this section, we conduct sensitivity analysis on the pore radius of the large-pore system. Using a similar approach to the last section, we run three cases, the properties of which are listed in Table 4. The permeability multiplier with respect to reservoir pressure of the three different types of larger pores is shown in Fig. 13. From Table 4 and Fig. 13, we can see that the apparent permeability enhancement effects and adsorption effects are not as significant on the large-pore system compared the small-pore system. The pore radius has influence mostly on the absolute permeability of the rocks.

The methane production rate and the cumulative production curves are shown in Fig. 14 and Fig. 15 respectively. According to the two figures, the pore radius of the large-pore system impacts the early stage of production. The three production curves deviate from each other at the start of the production time. After certain time of production, the production rate of the three cases becomes similar, indicating that after the depletion of the initial gas inside the fracture and the larger pores, the smaller pores start to become the major source of the production. From this sensitivity analysis, we can draw the conclusion that the large-pore system affects the early stage of the production by controlling the absolute permeability.

4.4. Sensitivity analysis of adsorption capability

In this section we conduct sensitivity analysis on the adsorption capability of the shale formation by using different Langmuir volumes for the small-pore system and investigating its effects on production. The parameters used this sensitivity analysis are listed in Table 5. Those parameters not listed in Table 5 are the same as those of the base case as shown in Table 1. The methane production rate and the cumulative production curves are shown in Fig. 16 and Fig. 17 respectively. As shown by the two figures, adsorbed gas starts to affect the production at the late stage of the production, after depletion of the fractures and the larger pores. The Langmuir volume directly affects the total amount of gas produced. By comparing Figs. 17 and 12, we can see that both adsorption

Table 4
Parameters related to pore radius for the large-pore system.

Case index	Pore radius	Absolute permeability	Langmuir volume
8	20 nm	6 μd	3 scf/ton
9	25 nm	10 μd	2.4 scf/ton
10	30 nm	14 μd	2 scf/ton

Please cite this article in press as: Wang, S., et al., The impact of kerogen properties on shale gas production: A reservoir simulation sensitivity analysis, Journal of Natural Gas Science and Engineering (2017), http://dx.doi.org/10.1016/j.jngse.2017.06.009

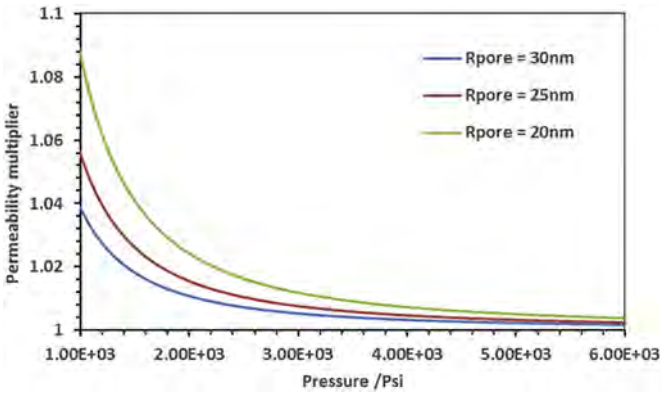

Fig. 13. Permeability multiplier for different larger pore radius.

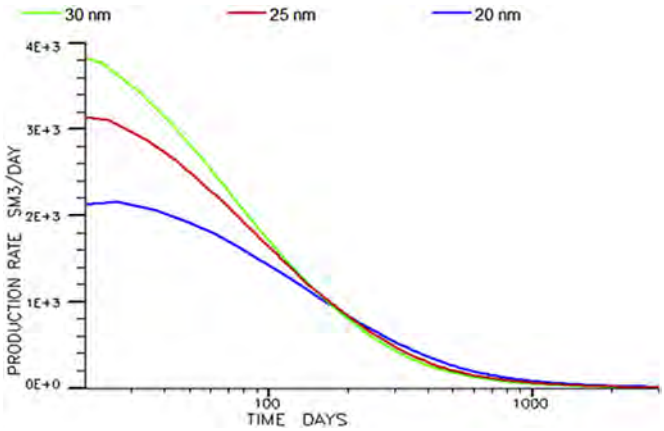

Fig. 14. Methane production rate with respect to time for different radius of the larger pores.

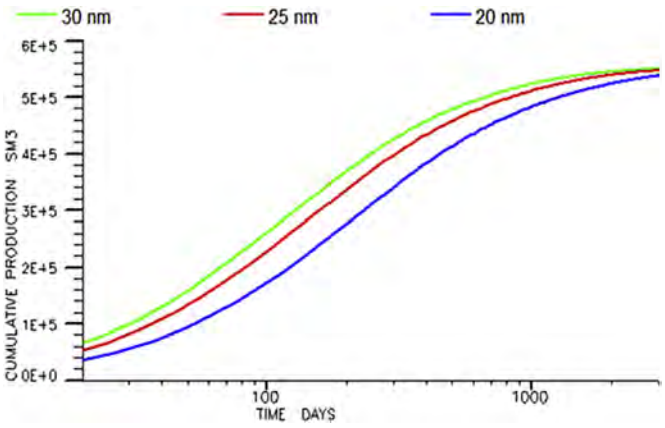

Fig. 15. Methane cumulative production with respect to time for different radius of the larger pores.

Table 5
Parameters for sensitivity analysis of adsorption capability.

Case index	Langmuir volume
11	40 scf/ton
12	28 scf/ton
13	16 scf/ton

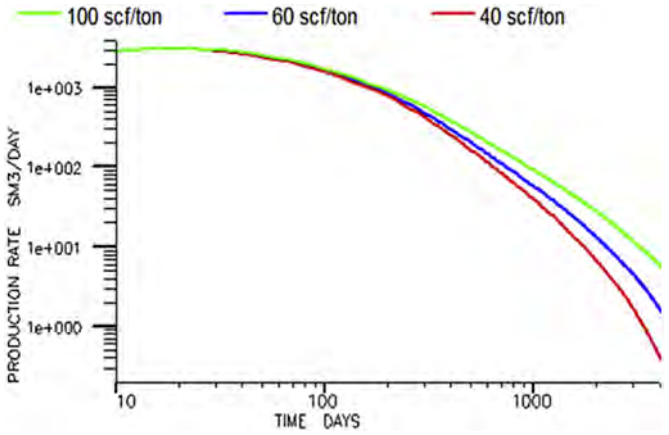

Fig. 16. Methane production rate curves with different Langmuir volume.

capability and small-pore radius affects the late stage of production. The difference is that the adsorption capability may have a more significant effect on the production rate (see Table 6)

4.5. Sensitivity analysis of the shape factors

As mentioned in the preceding chapters, the shape factor is an important concept in a multi-porosity approach. The shape factor is a parameter representing the conductivity between two porosity systems. In the formulation of the shape factor, the characteristic length is the most critical parameter. In this section, we conduct sensitivity analysis on both of the two shape factors used in the triple porosity approach. We aim to qualitatively determine the scale of the characteristic length. In this section, if not mentioned, the input parameters are chosen as those shown in Table 1.

4.5.1. Shape factor between the large-pore system and the small-pore system

We firstly investigate the shape factor between the large-pore system and the small-pore system. In this section, we test the sensitivity of the results on this characteristic length. We run two cases. The characteristic length of Case 14 and Case 15 is 1 μm and 0.1 μm respectively. Therefore, according to Equation (3.2), the shape factor of Case 15 is 100 times larger than that of Case 14. The results are shown in Fig. 18 and Fig. 19. According to the production rate curves shown in Fig. 18, the results of the two cases are very close to each other. This means that the shape factor is so large that the gas molecules inside the small-pore system can easily flow into the large-pore system. Therefore, although the permeability of the small-pore system is very low, the conductivity between the large-pore system and the small-pore system is still relatively high, causing the production to be essentially insensitive to the characteristic length in this range.

4.5.2. The shape factor between the large-pore system and the fracture

Since only the organic matter inside the shale matrix is permeable to gas, the shape factor between the large-pore system and the fracture shall be corrected by the volume of the permeable portion. In this work, the shape factor σ is corrected as shown in the following equation

$$\sigma = \left(\frac{V_p}{V_m}\right)\sigma_0 \tag{4.1}$$

where σ_0 is the original shape factor, V_p is the volume of the large-

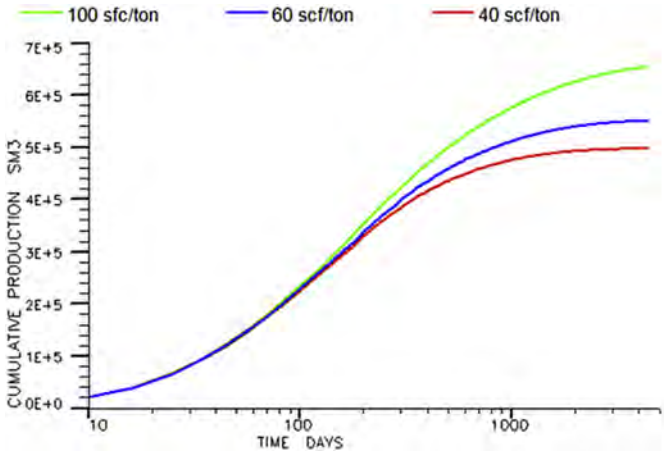

Fig. 17. Methane cumulative production curves with different Langmuir volume cumulative production.

Table 6
Parameters for sensitivity analysis of the shape factor between the large-pore system and the small-pore system.

Case index	Characteristic length	Langmuir volume
14	1 μm	60 scf/ton
15	0.1 μm	60 scf/ton

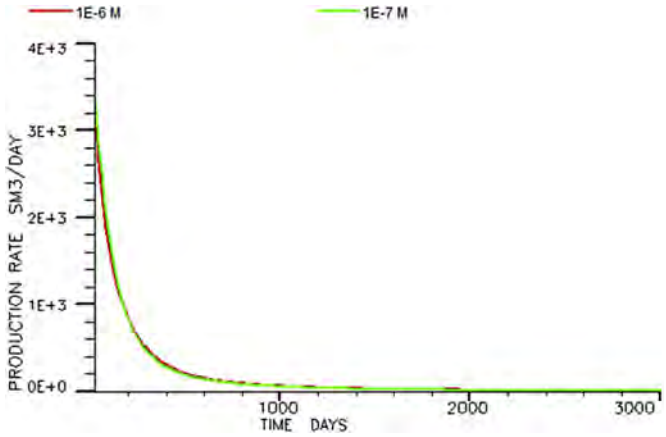

Fig. 18. Methane production rate of two different cases.

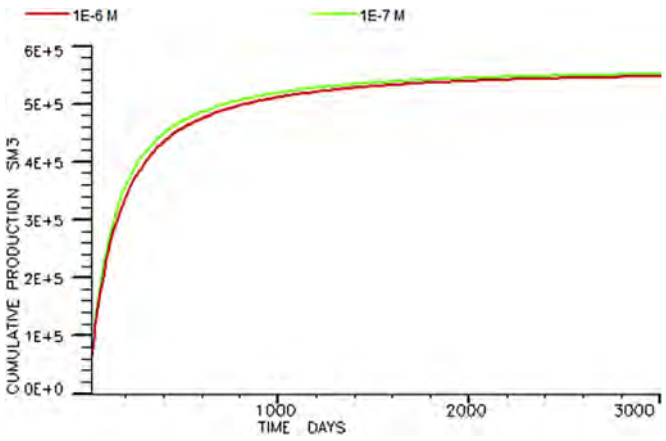

Fig. 19. Methane cumulative production of two different cases.

pore system and V_m is the total volume of the matrix block, as shown in Fig. 20. We compare cases with and without the volume correction. The results are shown in Fig. 21 and Fig. 22 respectively. The depletion time of the case with the volume correction is about 10 years, which is approximately 10 times of the case without the volume correction. In real reservoir production, the typical depletion time of shale reservoirs is also decades. Therefore, the results of the case with the volume correction is more reasonable.

5. Summary and conclusion

In this paper, we have combined the triple porosity model with recent advances in the study of kerogen structure, in particular the observation that kerogen contains both pores ~25 nm in size (as observed by SEM) and pores ~ 1 nm in size (as observed by X-ray and neutron diffraction). Here, the fractures in shale reservoirs as well as the large and small pores in kerogen are modeled as separate porosity systems. Sensitivity analysis are conducted on the pore radius, adsorption capability and shape factors that are used in the model. The conclusions from this study are as follows. Firstly, the larger kerogen-hosted pores, which contain free gas and are directly connected to the fracture system, impact the early stage of

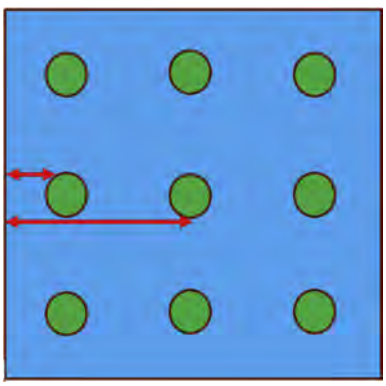

Fig. 20. Conceptual model showing the organic matter and surrounding fractures. The green part denotes the organic matter, while the blue part denotes the inorganic matter. The matrix rock consisting organic matter and inorganic matter is surrounded by the fractures. (For interpretation of the references to colour in this figure legend, the reader is referred to the web version of this article.)

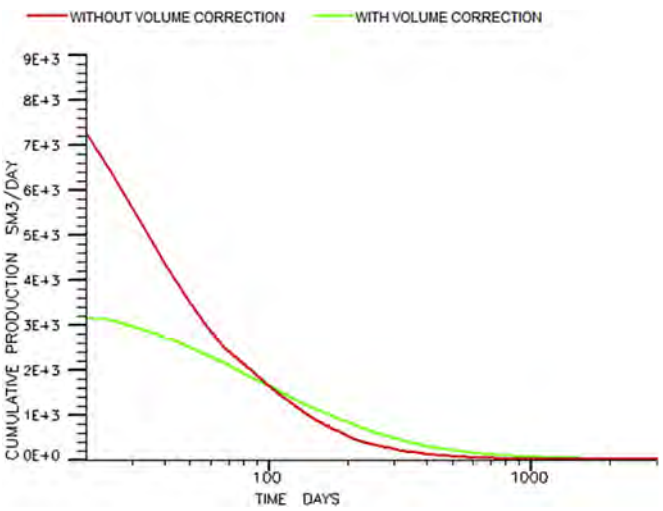

Fig. 21. Methane production rate curves with and without the correction of the shape factor.

Please cite this article in press as: Wang, S., et al., The impact of kerogen properties on shale gas production: A reservoir simulation sensitivity analysis, Journal of Natural Gas Science and Engineering (2017), http://dx.doi.org/10.1016/j.jngse.2017.06.009

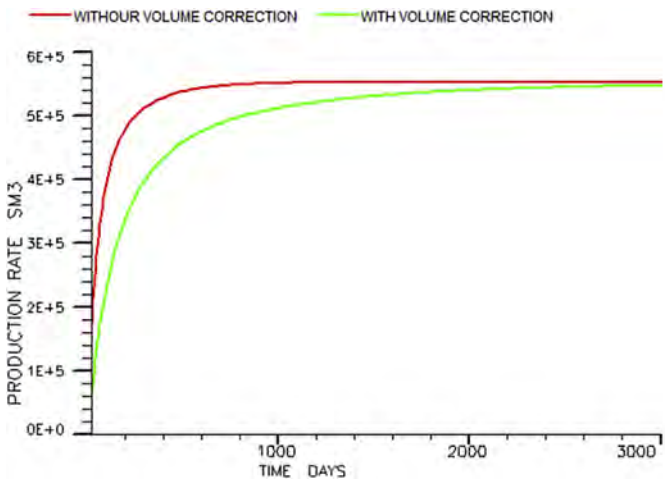

Fig. 22. Cumulative production curves with and without the correction of the shape factor.

the production. On the other hand, the smaller kerogen-hosted pores, which contain primarily adsorbed gas and are connected to the fracture system through the larger kerogen-hosted pores, impact the late stage of the production. Significant production from the smaller pores occurs only after the reservoir pressure has dropped and the larger pores are significantly depleted. Secondly, the shape factor significantly affects the results. The shape factor between the larger pores and the fractures determines the length of the reservoir depleting time, while the shape factor between the larger pores and the smaller pores determines the time when adsorbed gas starts to impact the production. Therefore, the characteristic length used in the shape factor should be carefully determined in any future studies. Thirdly, the pore radius effects both the production rate and the cumulative production. The radius of the larger pores impacts mostly the absolute permeability and therefore the rate of production, particularly for early production. The radius of the smaller pores impacts the adsorption capacity and therefore the cumulative gas production. However, the small pore system has such low permeability that variations in the permeability associated with variations in the pore size do not significantly influence the production. We should emphasize that in our model, the matrix rock is inside the SRV and is highly fractured. Therefore, each rock block has direct connection with the main fracture system. For matrix that is outside the SRV or without natural fracture networks, the model can also be modified to simulate double porosity system.

Nomenclature

A	interface area
D_0	Knudsen diffusion coefficient
F	flux term
G	gravity terms
K	component index
K_0	absolute permeability
K_a	apparent permeability
K_N	Knudsen number
L	characteristic length
M	accumulation term
M	molecular weight
m_a	adsoprtion mass
N	number of fracture sets
Q	generation term
P	pore pressure
P_L	Langmuir pressure
R	pore radius
r_0	reference pore radius
S	permeability multiplier
T	time
V	volume
V_L	Langmuir volume
V_{L0}	reference Langmuir volume
B	phase index
μ	viscosity
Δ	collision diameter
Λ	mean free path
ρ	density
Σ	shape factor
σ_s	tangential accommodation momentum coefficient (TMAC)
$\varnothing$	porosity

References

Agrawal, A., Prabhu, S.V., 2008. Survey on measurement of tangential momentum accommodation coefficient. J. Vac. Sci. Technol. A Vac. Surfaces, Films 26 (4), 634. http://doi.org/10.1116/1.2943641.

Aguilera, R., 2002. Incorporating capillary pressure, pore throat aperture radii, height above free-water table, and Winland r35 values on Pickett plots. AAPG Bull. 86 (4), 605–624.

Ambrose, R.J., Hartman, R.C., Diaz-Campos, M., Akkutlu, I.Y., Sondergeld, C.H., 2012. Shale gas-in-place calculations Part I: new pore-scale considerations. SPE J. 17 (1), 219–229. http://doi.org/10.2118/131772-PA.

Ambrose, R.J., Hartman, R.C., Diaz Campos, M., Akkutlu, I.Y., Sondergeld, C., 2010. New pore-scale considerations for shale gas in place calculations. In: SPE Unconventional Gas Conference. Society of Petroleum Engineers. http://doi.org/10.2118/131772-MS.

Bousige, C., Ghimbeu, C.M., Vix-Guterl, C., Pomerantz, A.E., Suleimenova, A., Vaughan, G., Coasne, B., 2016. Realistic molecular model of kerogen's nanostructure. Nat. Mater. 15 (5), 576–582. http://doi.org/10.1038/nmat4541.

Chew, A.D., 2009. Comment on "survey on measurement of tangential momentum accommodation coefficient". J. Vac. Sci. Technol. A Vac. Surfaces, Films 27 (3), 591 [J. Vac. Sci. Technol. A 26, 634(2008)]. http://doi.org/10.1116/1.3106613.

Cipolla, C.L., Lolon, E.P., Erdle, J.C., Rubin, B., 2010. Reservoir modeling in shale-gas reservoirs. SPE Reserv. Eval. Eng. 13 (4), 638–653. http://doi.org/10.2118/125530-PA.

Curtis, M.E., Ambrose, R.J., Sondergeld, C.H., 2010. Structural characterization of gas shales on the micro- and nano-scales. In: Canadian Unconventional Resources and International Petroleum Conference. Society of Petroleum Engineers. http://doi.org/10.2118/137693-MS.

Ertekin, T., King, G.A., Schwerer, F.C., 1986. Dynamic gas slippage: a unique dual-mechanism approach to the flow of gas in tight formations. SPE Form. Eval. 1 (1), 43–52. http://doi.org/10.2118/12045-PA.

Falk, K., Coasne, B., Pellenq, R., Ulm, F.-J., Bocquet, L., 2015. Subcontinuum mass transport of condensed hydrocarbons in nanoporous media. Nat. Commun. 6 (6949). http://doi.org/10.1038/ncomms7949.

Gensterblum, Y., Ghanizadeh, A., Cuss, R.J., Amann-Hildenbrand, A., Krooss, B.M., Clarkson, C.R., Zoback, M.D., 2015. Gas transport and storage capacity in shale gas reservoirs – a review. Part A: transport processes. J. Unconv. Oil Gas Resour. 12, 87–122. http://doi.org/10.1016/j.juogr.2015.08.001.

Heller, R., Zoback, M., 2014. Adsorption of methane and carbon dioxide on gas shale and pure mineral samples. J. Unconv. Oil Gas Resour. 8, 14–24. http://doi.org/10.1016/j.juogr.2014.06.001.

Ho, T.A., Criscenti, L.J., Wang, Y., 2016. Nanostructural control of methane release in kerogen and its implications to wellbore production decline. Sci. Rep. 6 (28053). http://doi.org/10.1038/srep28053.

Jarvie, D.M., Hill, R.J., Ruble, T.E., Pollastro, R.M., 2007. Unconventional shale-gas systems: the mississippian barnett shale of north-central Texas as one model for thermogenic shale-gas assessment. AAPG Bull. 91 (4), 475–499. http://doi.org/10.1306/12190606068.

Kazemi, H., Merrill, L.S., Porterfield, K.L., Zeman, P.R., 1976. Numerical simulation of water-oil flow in naturally fractured reservoirs. Soc. Petroleum Eng. J. 16 (6), 317–326. http://doi.org/10.2118/5719-PA.

Kleinstreuer, C., Koo, J., 2004. Computational analysis of wall roughness effects for liquid flow in micro-conduits. J. Fluids Eng. 126 (1), 1. http://doi.org/10.1115/1.1637633.

Knudsen, M., 1909. Die Gesetze der Molekularströmung und der inneren Reibungsströmung der Gase durch Röhren. Ann. Der Phys. 333 (1), 75–130. http://doi.org/10.1002/andp.19093330106.

Knudsen, M., 1934. The Kinetic Theory of Gases. Methuen & Co. Ltd, London.

Langmuir, I., 1918. The adsorption of gases on plane surfaces of glass, mica and platinum. J. Am. Chem. Soc. 40 (9), 1361–1403. http://doi.org/10.1021/ja02242a004.

Please cite this article in press as: Wang, S., et al., The impact of kerogen properties on shale gas production: A reservoir simulation sensitivity analysis, Journal of Natural Gas Science and Engineering (2017), http://dx.doi.org/10.1016/j.jngse.2017.06.009

Li, X., Abass, H., Teklu, T.W., Cui, Q., 2016. A shale matrix imbibition model – interplay between capillary pressure and osmotic pressure. In: SPE Annual Technical Conference and Exhibition. Society of Petroleum Engineers. http://doi.org/10.2118/181407-MS.

Lim, K.T., Aziz, K., 1995. Matrix-fracture transfer shape factors for dual-porosity simulators. J. Petroleum Sci. Eng. 13 (3), 169–178. http://doi.org/10.1016/0920-4105(95)00010-F.

Maxwell, C., 1879. On stresses in rarified gases arising from inequalities of temperature on JSTOR. Philosophical Trans. R. Soc. Lond. 170, 231–256. http://doi.org/10.1098/rstl.1879.006.

Peng, D.-Y., Robinson, D.B., 1976. A new two-constant equation of state. Industrial Eng. Chem. Fundam. 15 (1), 59–64. http://doi.org/10.1021/i160057a011.

Present, R.D., 1958. Kinetic Theory of Gases. Retrieved from. McGraw-Hill. https://scholar.google.com/scholar?hl=en&q=kinetic+theory+of+gases+present&btnG=&as_sdt=1%2C6&as_sdtp=.

Pruess, K., 1985. A practical method for modeling fluid and heat flow in fractured porous media. Soc. Petroleum Eng. J. 25 (1), 14–26. http://doi.org/10.2118/10509-PA.

Ralchenko, Y., Kramida, A., Reader, J., 2010. NIST Atomic Spectra Database (Version 4.0). Retrieved from. National Institute of Standards. http://www.nist.gov/manuscript-publication-search.cfm?pub_id=100132.

Sclumberger, 2010. ECLIPSE Reservoir Simulator, Manual and Technical Description. Google Scholar.

Tang, G.H., Tao, W.Q., He, Y.L., 2005. Gas slippage effect on microscale porous flow using the lattice Boltzmann method. Phys. Rev. E 72 (5), 56301. http://doi.org/10.1103/PhysRevE.72.056301.

Wang, S., Huang, Z., Wu, Y.-S., Winterfeld, P.H., Zerpa, L.E., 2016. A semi-analytical correlation of thermal-hydraulic-mechanical behavior of fractures and its application to modeling reservoir scale cold water injection problems in enhanced geothermal reservoirs. Geothermics 64, 81–95. http://doi.org/10.1016/j.geothermics.2016.04.005.

Wang, J., Dong, M., Yang, Z., Gong, H., Li, Y., 2017a. Investigation of methane desorption and its effect on the gas production process from shale: experimental and mathematical study. Energy & Fuels 31 (1), 205–216. http://doi.org/10.1021/acs.energyfuels.6b02033.

Wang, S., Lukyanov, A.A., Wang, L., Wu, Y.-S., Pomerantz, A., Xu, W., Kleinberg, R., 2017b. A non-empirical gas slippage model for low to moderate Knudsen numbers. Phys. Fluids 29 (1), 12004. http://doi.org/10.1063/1.4974319.

Wang, L., Wang, S., Zhang, R., Wang, C., Xiong, Y., Zheng, X., Rui, Z., 2017c. Review of multi-scale and multi-physical simulation technologies for shale and tight gas reservoirs. J. Nat. Gas Sci. Eng. 37, 560–578. http://doi.org/10.1016/j.jngse.2016.11.051.

Warren, J.E., Root, P.J., 1963. The Behavior of naturally fractured reservoirs. Soc. Petroleum Eng. J. 3 (3), 245–255. http://doi.org/10.2118/426-PA.

Xu, W., Diaz, C., Kadayam, V., 2015. Methods for Monitoring Fluid Flow and Transport in Shale Gas Reservoirs.

Yan, B., Alfi, M., An, C., Cao, Y., Wang, Y., Killough, J.E., 2016a. General Multi-Porosity simulation for fractured reservoir modeling. J. Nat. Gas Sci. Eng. 33, 777–791. http://doi.org/10.1016/j.jngse.2016.06.016.

Yan, B., Wang, Y., Killough, J.E., 2016b. Beyond dual-porosity modeling for the simulation of complex flow mechanisms in shale reservoirs. Comput. Geosci. 20 (1), 69–91. http://doi.org/10.1007/s10596-015-9548-x.

Yang, T., Li, X., Zhang, D., 2015. Quantitative dynamic analysis of gas desorption contribution to production in shale gas reservoirs. J. Unconv. Oil Gas Resour. 9, 18–30. http://doi.org/10.1016/j.juogr.2014.11.003.

Zhang, T., Ellis, G.S., Ruppel, S.C., Milliken, K., Yang, R., 2012a. Effect of organic-matter type and thermal maturity on methane adsorption in shale-gas systems. Org. Geochem. 47, 120–131. http://doi.org/10.1016/j.orggeochem.2012.03.012.

Zhang, W.M., Meng, G., Wei, X., 2012b. A review on slip models for gas microflows. Microfluid. Nanofluidics 13 (6), 845–882. http://doi.org/10.1007/s10404-012-1012-9.

Zhang, H., Zhang, Z., Ye, H., 2012c. Molecular dynamics-based prediction of boundary slip of fluids in nanochannels. Microfluid. Nanofluidics 12 (1–4), 107–115. http://doi.org/10.1007/s10404-011-0853-y.

Zimmerman, R.W., Chen, G., Hadgu, T., Bodvarsson, G.S., 1993. A numerical dual-porosity model with semianalytical treatment of fracture/matrix flow. Water Resour. Res. 29 (7), 2127–2137. http://doi.org/10.1029/93WR00749.

Please cite this article in press as: Wang, S., et al., The impact of kerogen properties on shale gas production: A reservoir simulation sensitivity analysis, Journal of Natural Gas Science and Engineering (2017), http://dx.doi.org/10.1016/j.jngse.2017.06.009